J Mater Sci (2011) 46:7725–7736
DOI 10.1007/s10853-011-5752-9

Chemical nano-scale homogeneity of austenitic CrMnCN steels in relation to electronic and magnetic properties

B. D. Shanina · A. I. Tyshchenko · I. N. Glavatskyy · V. V. Runov · Yu N. Petrov · H. Berns · V. G. Gavriljuk

Received: 24 March 2011 / Accepted: 27 June 2011 / Published online: 9 July 2011

Abstract Measurements of conduction electron spin resonance, temperature-dependent magnetization, small angle neutron scattering, and transmission electron microscopy were used for the analysis of chemical nonhomogeneity in austenitic steels with carbon + nitrogen or carbon only. It is shown that all studied steels are characterized by a nonhomogeneous distribution of alloying elements on the fine scale: from 3 to 5 nm in CrMnCN steels to about 30 nm in MnC Hadfield type steel. In the CN steels, their chemical homogeneity is improved by decreasing the C/N ratio. A ferromagnetic-type temperature behavior is observed in the CN steels at temperatures below 86 K, which is attributed to the blocking of magnetic moments of superparamagnetic clusters. The short-range decomposition of all studied steels results in a different splitting of dislocations, which corresponds to two different values of the stacking fault energy.

B. D. Shanina
Department of Optics and Spectroscopy, V. Ye Lashkarev Institute for Semiconductor Physics, 03028 Kiev, Ukraine

A. I. Tyshchenko · I. N. Glavatskyy · Y. N. Petrov · V. G. Gavriljuk (✉)
Department of Alloyed Steels, G.V. Kurdyumov Institute for Metal Physics, 03680 Kiev 142, Ukraine
e-mail: gavr@imp.kiev.ua

I. N. Glavatskyy
Institute for Complex Magnetic Materials, Helmholtz Centre Berlin for Materials and Energy, 14109 Berlin, Germany

V. V. Runov
Konstantinov St. Petersburg Nuclear Physics Institute, Gatchina, Russia 188350

H. Berns
Ruhr University Bochum, 44801 Bochum, Germany

Introduction

The correlation between atomic interaction and atomic distribution in iron-based alloys was the topic of studies [1–5]. It was shown that an enhanced metallic character of interatomic bonds, i.e. an increase in the concentration of conduction (free) electrons at the Fermi level assists short-range ordering in solid solutions, whereas covalent bonds promote clustering. In turn, the thermodynamic stability is increased if the distribution of solute atoms is characterized by a tendency toward atomic ordering and decreased if the solute atoms are prone to form clusters.

Comparative studies of martensitic chromium steels alloyed with nitrogen or carbon (see e.g. [3]) have shown that, in contrast to carbon, nitrogen increases the stability of austenite to martensitic transformation as well as the stability of martensite to precipitation during tempering. Thus, nitrogen is a stronger stabilizer of both austenitic and martensitic solid solutions. It was also found in these studies that alloying with nitrogen + carbon is most effective in stabilizing both, austenitic and martensitic solid solutions in relation to transformation and precipitation.

The present study is aimed at investigating in more detail the effect of the C + N concentration and, particularly, the C/N ratio on the electronic properties of chemical nonhomogeneities in the iron-based fcc solid solution. Along with the austenitic C + N steels, a Hadfield steel is taken for comparison.

The conduction electron spin resonance (CESR) allows to measure the concentration of conduction electrons in paramagnetic objects. At the same time, due to measurements of the *g*-factor (factor of splitting of the electron energy levels under an applied magnetic field) and the temperature dependence of the magnetic susceptibility, one can investigate the interaction between conduction and

localized electrons, which provides quantitative data about the fractions of single substitutional *d*-atoms and their superparamagnetic clusters, i.e. it allows to estimate the distribution of the transition metal atoms (Cr, Ni, Mn etc.) in the solid solution (see [2] for details).

The obtained CESR data on inhomogeneous concentrations were compared with those studied by small angle scattering of neutrons (SANS), magnetic measurements, and TEM studies of the stacking fault energy (SFE).

Experimental

The chemical composition of three CrMnCN steels and the Hadfield steel C1.2 is given in Table 1. The CrMnCN steels are designated by their C + N content. At an almost equal nitrogen content, the carbon content decreases from CN1.07 to CN0.85.

CrMnCN melts of 3 metric tons were poured to ingots and subsequently electro-slag-remelted and hot worked to Ø 125 mm. Specimens were taken in longitudinal direction at 2/3 radius by electro-sparc-erosion, solution annealed and quenched in water. The respective temperatures were 1,100 °C for CN0.85 and CN0.96, but 1,175 °C for CN1.07. After machining to final size, the light optical examination revealed a fully austenitic microstructure. The Hadfield steel was stemmed from 100 mm^2 square hot-worked stock. The respective specimens were quenched from 1,100 °C in water. Plates of 5 mm thickness were used for SANS. They were thinned to 65 μm thickness for CESR.

An electron paramagnetic resonance (EPR) spectrometer with a frequency $\nu = 9.3$ GHz, a microwave field power $P = 10$ dB, a modulating field with modulation amplitude $H_m = 2 \times 10^{-4}$ T and frequency $\nu_m = 10^5$ Hz was used for the measurements. The CESR signals were recorded within the temperature interval of 20–300 K. The resolution of the CESR spectra is determined by the quality of resonator, which affects the signal/noise ratio and can be decreased by metallic samples. It can be estimated from Fig. 1a, b. For steel CN0.85, the signal/noise ratio was about 5,000, which is very good, whereas in the case of measurements on steels CN1.07 and CN0.96 the noise was higher leading to a ratio of about 1,000 which is smaller but still allows to record the signal with sufficient accuracy.

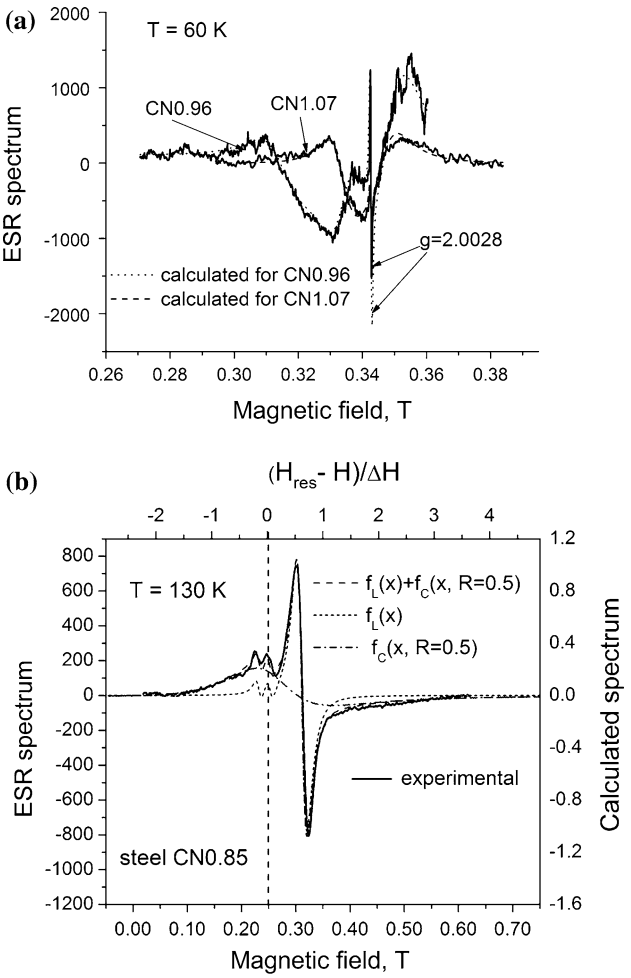

Fig. 1 ESR spectra of steels CN1.07, 0.96 (**a**) and CN0.85 (**b**)

The amplitude of signals was measured in relative units of the EPR intensity of the reference sample $I_0 = I_{ref}$ ($T = 1$ K). A piece of borate glass having 8×10^{14} spins was used as a reference sample for the determination of the free electron concentration. The neutron scattering measurements were carried out using the SANS facility "Vector" in the WWR-M reactor of the Nuclear Physics Institute at St. Petersburg, at a wave length of $\lambda = 9.2$ Å ($\Delta\lambda/\lambda = 0.25$). This instrument is equipped with a 20-counter (^{3}He) detector and a multichannel analyzer which operated in slit geometry within the momentum $q = 2\pi\theta/\lambda$ transfer range of 1.5×10^{-3} to 3×10^{-1} Å^{-1}

Table 1 Chemical compositions (mass%)

Elements steel	C	N	Cr	Mn	Ni	Si	Mo	C + N	C/N
CN1.07	0.489	0.578	18.8	18.9	0.40	0.43	0.07	1.07	0.85
CN0.96	0.344	0.614	18.2	18.9	0.34	0.30	0.06	0.96	0.56
CN0.85	0.256	0.596	18.3	18.4	0.10	0.54	0.02	1.07	0.43
C1.2	1.19	0.009	0.2	12.1	0.10	0.49	–	1.20	–

($\mathbf{q} = \mathbf{k} - \mathbf{k}'$, where $\mathbf{k}$, $\mathbf{k}'$ are the wave vectors of falling and scattered neutrons, respectively). The polarization of the falling beam was $P_0 = 92\%$. Measurements were performed at room temperature under zero magnetic field.

The Quantum Design Physical Properties Measurement System (PPMS-14T) with a maximum magnetic field of 14 T and a temperature range of 1.8 to 300 K was used for magnetic measurements.

Measurements of the dislocation triple node radius were used to determine the SFE according to the method described in [6]. For this the transmission electron microscope JEM-2000 FXII operating at a voltage of 200 kV was used. In each studied steel, about thirty to sixty triple nodes were investigated.

CESR results

CESR spectra

Figure 1 shows the spectra of the steels CN1.07, CN0.96, and CN0.85. One can see that the spectra of CN1.07 and CN0.96 are similar, whereas the spectrum of CN0.85 is quite different. At 60 K, the steels CN1.07 and CN0.96 give resonance signals of complex multiple structure (see Fig. 1a), indicating a submicron-inhomogeneous system. The measured samples have a high conductivity and decrease the quality of the resonator in the EPR spectrometer. For this reason, we needed to use a large amplification coefficient and take packets of two or several thin foils. The theoretical analysis of the spectra shows that they consist of two resonance signals with different phases: one signal has a zero phase and is related to the localized paramagnetic centers, the other signal has a 180°-phase and is related to conduction electrons. Both spectra were recorded under the same experimental conditions. The narrow line of extremely low integral intensity in the spectra of both steels has a factor of spectroscopic splitting (g-factor) $g = 2.0028$, which is specific for dangle carbon bonds. This can stem from the presence of small undissolved carbide particles in the matrix, which were not resolved in TEM studies. The part of the spectrum related to the conduction electrons is larger in CN0.96 than in CN1.07.

Figure 1b shows the CESR spectrum of steel CN0.85, recorded at $T = 130$ K. Like the spectra of CN0.96 and CN1.07, this spectrum consists of two main components. One wide spectral line has an asymmetrical line-shape, a so-called Dyson line-shape, typical for free electron spin resonance in samples of thickness $d > \delta$, where δ is the skin layer depth. The second spectral line is a narrow signal with a Lorentz line-shape which is typical for localized paramagnetic centers (PC1). Besides this, two very small lines are observed at the left wing of the PC1 signal. They look like a superfine splitting of the resonance signal, which belongs to other localized centers PC2 with a nuclear spin of $I = 1/2$. The iron isotope Fe^{57} is the only element in the studied alloy having nuclei with a spin of $I = 1/2$. We did not analyze these lines because they were too small. Possibly, because of their small value and the low signal/noise ratio, they were not observed in the samples CN0.96 and CN1.07.

Temperature dependence of the resonance spectra

As an example, the resonance signals from steel CN1.07 observed at temperatures of 20 K $< T <$ 140 K are presented in Fig. 2. Figure 3a, b presents spectra from steel CN0.85 measured in two temperature ranges. The spectrum at $T = 320$ K (see Fig. 3a) was recorded simultaneously with the CESR signal of the reference sample, which is seen at a magnetic field of $H = 0.16$ T.

Starting from 85 K, a reversible phase transformation is observed from paramagnetic to some new magnetic state within a temperature range of about 3 K (Fig. 3b). The absorption signal is very intensive and looks like a ferromagnetic absorption. It increases and broadens if the temperature decreases to 83 K. At temperatures below 83 K, the signal is not remarkably changed, the spectral line of conduction electrons disappears, the narrow line of the localized paramagnetic centers decreases and can be observed in the background of this broad signal.

This transformation may indicate the transition from a paramagnetic to a ferromagnetic state or to blocked magnetic moments of superparamagnetic clusters, which is discussed in Sect. 4 where the measurements of static magnetization are described.

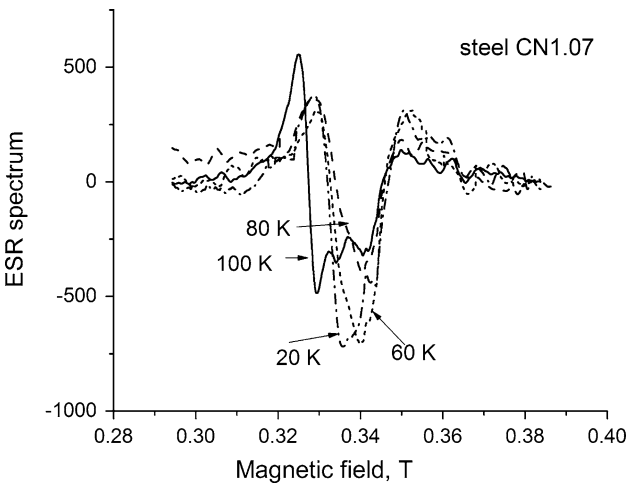

Fig. 2 ESR spectra of steel CN1.07 measured at different temperatures

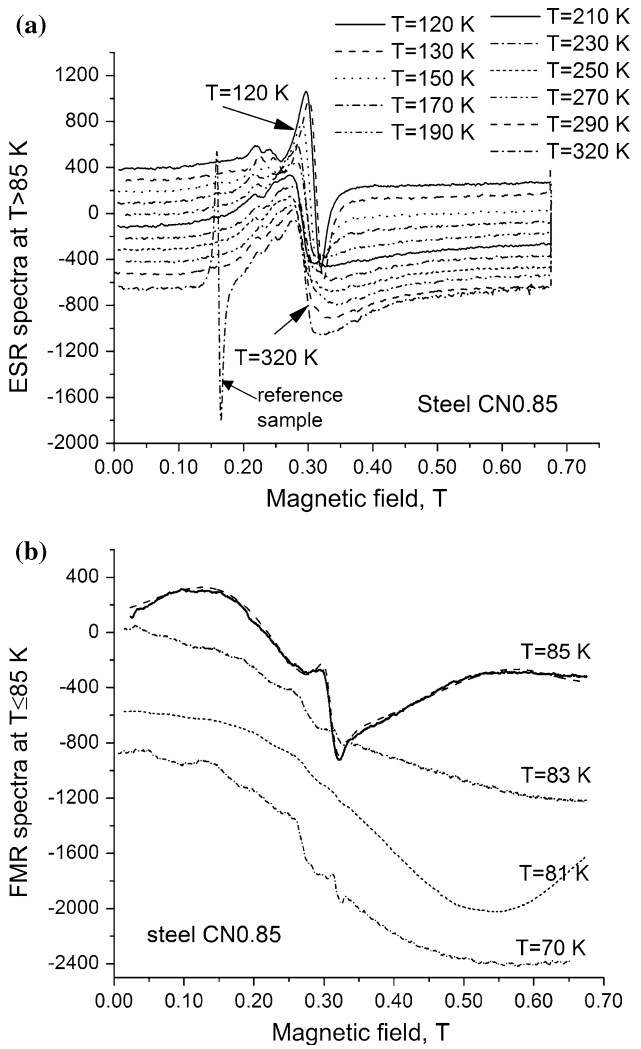

Fig. 3 Temperature behavior of ESR spectra in steel CN0.85 above 85 K (**a**) and magnetic resonance in CN0.85 at temperatures ≤85 K (**b**)

Analysis of spectral characteristics

The analysis of the paramagnetic spin resonance spectra of each temperature measured was carried out within the range of 20–140 K for steel CN1.07 and of 86–320 K for steel CN0.85. For steel CN0.96, we used the spectrum obtained at $T = 60$ K in comparison with the spectrum of CN1.07 at the same temperature.

The experimental EPR lines were described by the calculated derivative of the Lorentz function

$$f_L(x) = dL(x)/dx = -2A \cdot x/\left(1 + x^2\right)^2, \quad (1)$$

where $x = (H_{res} - H)/\Delta H$, H is the magnetic field and H_{res} is the value of the resonance magnetic field which is determined from the condition $f_L(x) = 0$.

The signal of conduction electrons is described by the calculated derivative of the ESR signal. The latter is a function of x and the parameter $R = \delta^2/\delta_e^2$, where δ is the skin layer depth and δ_e is the diffusion length of the electron for the spin relaxation time.

Using the theoretical function given in [1, 7], the theoretical curves of the derivative of the CESR signal lineshape $f_C(x,R)$ were calculated for different R values within the range of 0.01–10. The obtained curves were used to fit $f_L(x) + f_C(x,R)$ to the experimental spectra. For all CN0.1.07 and CN0.96 spectra, $R = 0.5$ was found, whereas R changed from 0.5 at $T = 100$ K to 1.0 at $T = 270$ K for steel CN0.85. As will be shown further in Sects. 3.3.1 and 3.3.2 (see also Table 2), the increase of R in steel CN0.85 is due to a stronger scattering of free electrons on paramagnetic centers as well as superparamagnetic clusters. At $T \geq 290$ K, the CESR signal of CN0.85 became symmetrical and was described by the $f_L(x)$ function, indicating the skin layer depth to increase up to the sample thickness $d = 65$ μm. Figure 1b shows the result of fitting the calculated sum of two functions $f_L(x)$ and $f_C(x,R = 0.5)$ at $T = 130$ K.

The spectra of the samples CN0.1.07 and CN0.96 consist of the signal from localized spins of phase $\phi = 0$ and $f_C(x; R = 0.5)$ with a phase of 180°. Such a phase is typical for CESR of the conduction electron subsystem if the conditions of a "phonon bottleneck" are broken, i.e. the exchange interaction between conduction electrons and localized paramagnetic centers is small and, correspondingly, two signals are observed separately.

As a result of the analysis, the main parameters of the resonance signals (the resonance magnetic field for two signals $H_{res,1}$ and $H_{res,2}$, the line-widths ΔH_1 and ΔH_2, the integral intensities I_1 and I_2) were determined from the fitting and will be discussed in Sects. 3.3.1 and 3.3.2.

Concentration of conduction and localized electrons

The temperature dependence of integral signal intensities is estimated after double integration and compared with the reference sample containing 8×10^{14} spins. The values I_e, I_{loc} are the resonance integral signal intensities of conduction electrons and of localized centers, respectively. I_0 stands for the integral intensity of the ESR signal of the reference sample reduced to $T = 1$ K. Its temperature dependence is described by the Curie–Weiss law, $I_{ref} = I_0/T$. Functions $I_e(T)/I_0$ and $I_{loc}(T)/I_0$ are presented by scatters

Table 2 Characteristics of paramagnetic systems

Steel	N_e, 10^{22} cm^{-3}	N_{loc}, 10^{18} cm^{-3}	χ_P, 10^{-7}	C, 10^{-6} K	α, 10^6	θ_p, K
CN1.07	2.0	1.0	3.04	0.77	−1.42	−131.5
CN0.96	2.9	0.77	4.41	0.55	–	−74
CN0.85	2.8	1.5	4.26	0.93	–	86

of the steels CN1.07, CN0.96 in Fig. 4a and of CN0.85 in Fig. 4b.

The integral intensity of the resonance signal from conduction electrons is mainly determined by the Pauli magnetic susceptibility which does not depend on temperature. However, I_e contains a small additive contribution depending on I according to the Curie–Weiss law, which is due to spin cross-relaxation caused by the exchange interaction between free electrons and localized centers. Particularly, this contribution occurs in steel CN1.07 and is too small to be observed in steels CN0.96 and CN0.85.

The curves shown by lines in Fig. 4a, b are calculated according to the following equations:

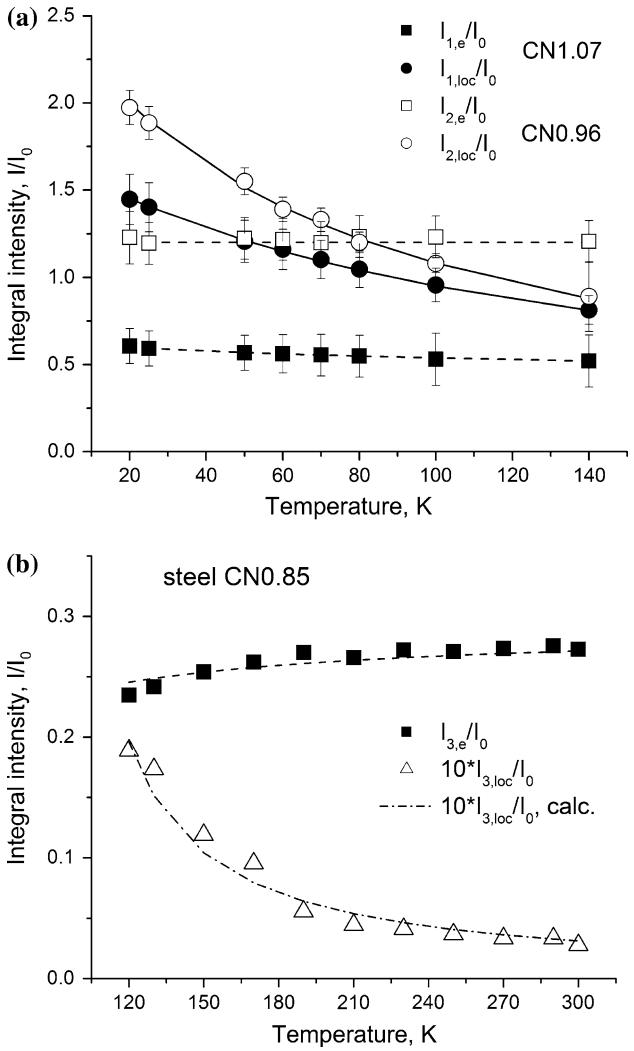

Fig. 4 Temperature dependence of the integral intensitiesof the EPR signals from conduction electrons (I_e/I_0) and localized centers (I_{loc}/I_0) in steels CN1.07, CN0.96 (**a**), and CN0.85 (**b**). The values calculated using Eq. 2a are presented by *dashed lines*

$$\text{for CN1.07}: I_{e,1}/I_0 = 0.423 + 26.5/(T + 131.5); \quad I_{loc,1}/I_0 = 220/(T + 131.5) \tag{2a}$$

$$\text{for CN0.96}: I_{e,2}/I_0 = 1.2; \; I_{loc,2}/I_0 = 188/(T + 74) \tag{2b}$$

$$\text{for CN0.85}: I_{e,3}/I_0 = 0.27; \; I_{loc,3}/I_0 = 0.67/(T - 86) \tag{2c}$$

These curves describe the experimental data satisfactorily. It follows from (2a) that $I_{e,1}/I_0 = 3.2$. Now we can estimate the conduction electron concentration in the samples CN1.07, CN0.96, and CN0.85 of volume V:

$$N_e = (8/9) \cdot (g_{ref}/g_e)^2 (I_e/I_0) \cdot (E_F/k) \cdot [S(S+1)] \cdot N_{ref}/V = 2.47 \cdot 10^{20} \cdot (I_e/I_0)/V. \tag{3}$$

For paramagnetic centers in the borate glass reference sample, we have $g_{ref}/g_e = 1.94$ and spin $S = 1/2$. E_F is the Fermi energy, k is the Boltzmann constant, $I_{e,1}/I_0 = 0.423$; $I_{e,2}/I_0 = 1.2$; $I_{e,3}/I_0 = 0.28$; $(E_F/k) = 1.23 \times 10^5$ at $T = 1$ K; $V_{CN1.07} = 0.0052$ cm^3, $V_{CN0.96} = 0.0104$ cm^3, $V_{CN0.85} = 0.0024$ cm^3.

Thus, the concentration of conduction electrons N_{ce} in samples CN1.07, CN0.96, and CN0.85 is equal to 2.0×10^{22}, 2.9×10^{22}, and 2.8×10^{22}, respectively.

The Eqs. 2a–c also allow to obtain the concentration of localized paramagnetic centers. At $T = 1$ K, we find:

$$I_{loc}(\text{CN1.07})/I_0 = 1.66; \; I_{loc}(\text{CN0.96})/I_0 = 2.5. \tag{4}$$

For steel CN0.85, we take this ratio at $T = 100$ K, i.e. sufficiently far away from the transformation temperature:

$$I_{loc}(\text{CN0.85; 100 K})/I_{ref}(\text{100 K}) = 100 \cdot I_{loc,3}/I_0 = 4.8. \tag{5}$$

Therefore, the concentration of localized paramagnetic centers in the samples is:

$$N_{loc}(\text{CN1.07}) = 1.66 \cdot 4 \cdot 8 \cdot 10^{14}/V_{CN1.07} = 1.0 \cdot 10^{18}\ \text{cm}^{-3};$$
$$N_{loc}(\text{CN0.96}) = 2.5 \cdot 4 \cdot 8 \cdot 10^{14}/V_{CN0.96} = 0.77 \cdot 10^{18}\ \text{cm}^{-3};$$
$$N_{loc}(\text{CN0.85}) = 4.8 \cdot 4 \cdot 8 \cdot 10^{14}/V_{CN0.85} = 1.5 \cdot 10^{18}\ \text{cm}^{-3}. \tag{6}$$

The Curie–Weiss constant can be calculated according to the known formula:

$$C_{CN1.07} = g^2\beta^2 S(S+1) \cdot N_{loc}/(3k_B) = 0.77 \cdot 10^{-6}; C_{CN0.96} = 0.55 \cdot 10^{-6}\ \text{K}; C_{CN0.85} = 0.93 \cdot 10^{-6}\ \text{K}. \tag{7}$$

The obtained spin concentrations allow to find the Pauli paramagnetic susceptibility of the conduction electron spin

subsystem, $\chi_P = 0.5\ g^2(\mu_B^2 D(E_F) = (3/8)\cdot 5\ g^2(\mu_B^2 N_e/E_F)$ which is given in Table 2.

Resonance fields

Figure 5a shows the temperature dependence of the resonance fields of conduction electrons and of localized paramagnetic centers (localized electrons) in steel CN1.07. Two paramagnetic subsystems, conduction electrons and localized spins of the host atoms in the metallic alloys, connect each other due to the exchange interaction. It is shown in [8] that, if the cross-relaxation is quicker than the spin-phonon relaxation of the conduction electron spin subsystem, the large exchange interaction causes an intensive cross-relaxation between two spin subsystems and a "phonon bottleneck". In this case, the magnetizations of both subsystems are united and we observe only one ESR signal with properties depending on the characteristics of both subsystems. This is the usual situation in iron-based alloys (see e.g. [2, 4]).

However in steel CN1.07, we observe two separated subsystems and, therefore, a "broken bottleneck" occurs and the rate of spin-phonon relaxation is higher than that of the cross-relaxation. Nevertheless, the exchange interaction between the two subsystems occurs and results in a temperature dependence of the resonance fields depending on the magnetic susceptibility of the second subsystem.

The following equations describe the experimental temperature dependence of the resonance magnetic field:

$$H_{\mathrm{res,e}}(\mathrm{CN1.07}) = H_{0,\mathrm{e}}\left[1 + \alpha \cdot C/\left(T - \theta_{\mathrm{p}}\right)\right]; \quad H_{0,\mathrm{e}} = 3475.8\ \mathrm{G};\ \alpha \cdot C = -1.094;\ \theta_{\mathrm{p}} = -131.5\ \mathrm{K}. \tag{8a}$$

$$H_{\mathrm{res,loc}}(\mathrm{CN1.07}) = \left(H_{0,\mathrm{loc}} + \left(T - \theta_{\mathrm{p}}\right)\cdot H_{0,\mathrm{e}} \cdot \chi_P^{(1)}/C\right)/ \times \left(1 + \left(T - \theta_{\mathrm{p}}\right)\cdot \chi_P^{(1)}/C\right); \quad H_{0,\mathrm{loc}} = 3275\ \mathrm{G};\ H_{0,\mathrm{e}} = 3475.8\ \mathrm{G};\ \chi_P^{(1)}/C = 2.5\cdot 10^{-3}. \tag{8b}$$

H_{0e}, $H_{0,\mathrm{loc}}$ are the values of the resonance magnetic fields of the conduction electron and the localized spin subsystems in absence of a second spin subsystem; α is a dimensionless parameter of the exchange interaction between two subsystems; C is the Curie–Weiss constant for paramagnetic susceptibility of localized spins $\chi_{\mathrm{C-W}}$; θ_{p} is the paramagnetic temperature in the Curie–Weiss law for $\chi_{\mathrm{C-W}}(T) = C/(T - \theta_{\mathrm{p}})$; χ_P is the Pauli paramagnetic susceptibility of the conduction electron subsystem.

The sign and value of θ_{p} characterize the exchange interaction between the localized spins. In this steel, the host atoms having spins are bound by the antiferromagnetic exchange interaction, the value of which is about 0.01 eV ($\theta_{\mathrm{p}} = -131.5$ K).

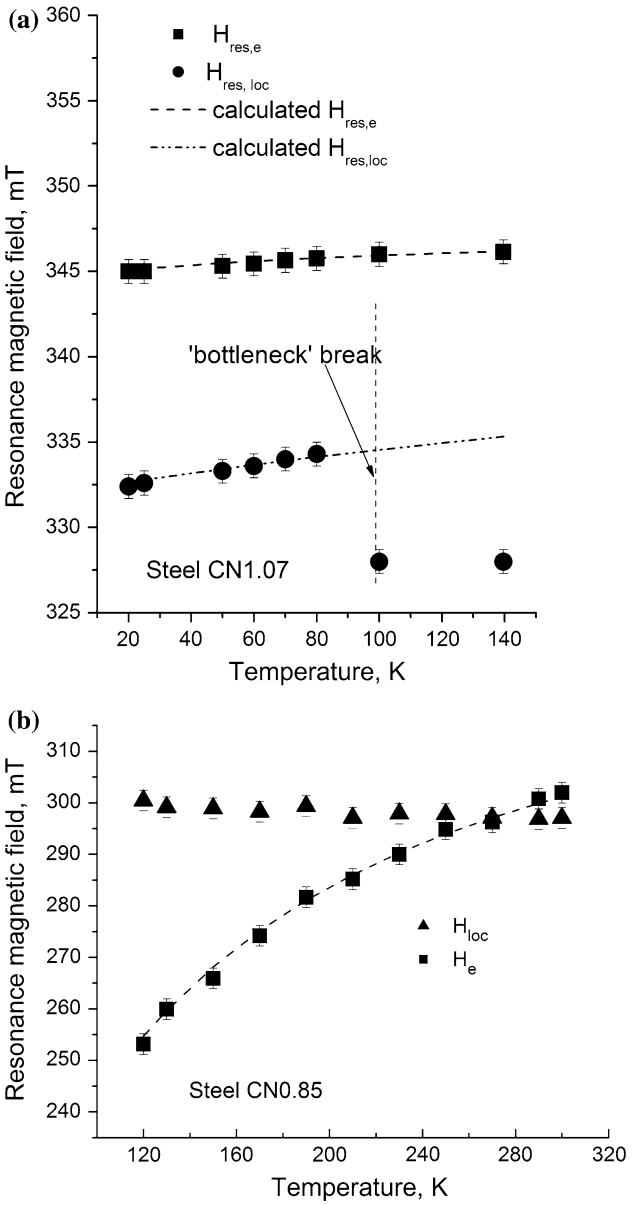

Fig. 5 Resonance magnetic fields of the EPR signals of conduction electrons and localized centers in CN1.07 (**a**) and CN0.85 (**b**). The *dashed lines* represent the values calculated using Eq. 8a

Equation 8a describes the contribution of the local exchange field from the localized spin subsystem to the resonance field of conduction electrons. This contribution is proportional to the exchange interaction between the conduction electrons and the localized spins and to the paramagnetic susceptibility of the localized spin subsystem.

Equation 8b describes the temperature dependence of the resonance magnetic field of the ESR signal of the localized spins. It is a known expression for the resonance field of a spin system bound with other spin system by the exchange interaction [9]. The fact that Eq. 8b well

describes the experimental data of the localized spin subsystem confirms that the latter interacts with a part of the conduction electron subsystem which is under conditions of the "bottleneck". As follows from Table 2, this fraction of conduction electrons is small because $\chi_P{}^{(1)}/C = 2.5 \times 10^{-3} << \chi_P/C$.

The temperature dependence of the resonance magnetic field for CESR in steel CN0.85 is presented in Fig. 5b. It demonstrates a strong influence of some superparamagnetic inclusions in the sample which cause local magnetic fields on the conduction electrons. The temperature dependence of $H_{res,e}$ for conduction electrons is described by the temperature function of the local magnetic field caused by superparamagnetic clusters, i.e. by the Langevin function $L = \coth(\theta/T) - T/\theta$:

$$H_{res,e} = H^{(0)}_{res,e} - B \cdot (\coth(\theta/T) - T/\theta). \quad (9)$$

Here, $H^{(0)}_{res,e}$ is the resonance magnetic field for CESR in the Fe-based alloys in the absence of any internal local magnetic field; $B = 4\pi M_{cl}$ is the maximum local magnetic field caused by a system of superparamagnetic clusters with a magnetic moment M; θ is the energy of an individual superparamagnetic cluster in the temperature units of which the magnetic moment under external magnetic field H is M:

$$\theta = MH/k_B = 2\mu_B HN/k_B, \quad (10)$$

where μ_B is the Bohr magneton, N is the number of spins in the cluster, and k_B is the Boltzmann constant.

The function (9) is shown in Fig. 5b by the dashed line with the following values: $H^{(0)}_{res,e} = 340$ mT; $B = 180$ mT; $\theta = 200$ K. By substituting θ in (10), the number of magnetic atoms in the cluster was estimated to be equal to about 500 atoms, which corresponds to an average cluster size of about 3 nm. Using the obtained $B = 180$ mT and $M = 0.92 \times 10^{-17}\text{erg}^{1/2}\,\text{cm}^{3/2}$, one can estimate the concentration of superparamagnetic clusters $n_{cl} = B/(4\pi M) = 1.55 \times 10^{19}\ \text{cm}^{-3}$. As only Mn can initiate the superparamagnetism in the studied steels, the obtained n_{cl} suggests that, in fact, all Mn atoms are involved in the formation of superparamagnetic clusters.

Thus, based on the obtained CESR spectra and their analysis, one can conclude that all studied steels have a high concentration of conduction electrons, which exceeds that in austenitic nitrogen steels without carbon (see e.g. [2, 4]). At the same time, along with the single paramagnetic centers of which the concentration N_{loc} is presented in Table 2, superparamagnetic clusters, i.e. clusters of substitutional solute atoms, exist in the studied steels. For steel CN0.85 their concentration is estimated at $1.55 \times 10^{19}\ \text{cm}^{-3}$ and their size at about 3 nm.

Magnetic measurements

To clarify the unusual behavior of the EPR spectra below 86 K and the magnetic nonhomogeneities, we measured the curves of static magnetization for steels CN0.85, CN1.07, and C1.2 within a wide range of magnetic field. The curves are given in Fig. 6a for steel CN0.85 at different temperatures and in Fig. 6b, c for steels CN1.07 and C1.2 at a temperature of 300 K. A feature of these data is the absence of magnetic saturation and the paramagnetic character of magnetization. In Fig. 6a, one can see a negligible temperature dependence of the magnetic moment. The magnetic moment M versus the magnetic field H can be satisfactorily described for all steels by a combination of a linear $M(H)$ function and the Langevin function $M = \text{const}\cdot(\coth(M_{cl}H/kT) - kT/M_{cl}H)$, which is typical for paramagnetism caused by superparamagnetic clusters.

For this reason, the curves in Fig. 6 were calculated using the function:

$$M = M_0 \cdot (\coth(H/H_0) - H_0/H) + H/H_1 \quad (11)$$

with parameters M_0, H_0, and H_1 presented in Table 3.

The constant M_0 is equal to $(g\mu_B N_{cl}/\rho)$, where N_{cl} is the concentration of clusters in the sample and ρ is the density of the alloy. The H_0 value in $L(H/H_0)$ is determined by $kT/(g\mu_B n_s)$, where n_s is the number of paramagnetic spins in a cluster. We suppose that all clusters have approximately the same size. The linear function versus H could be presented by the Curie–Weiss paramagnetic susceptibility, as well as by the Van Vleck atomic paramagnetism. In the case of C–W susceptibility, H_1 is determined from the Curie law and is equal to $4kT/g^2\mu_B^2 N_{PC}$. It depends on T linearly. The estimation of N_{PC} shows that a value of $H_1 = 7$ T would be obtained if the concentration of paramagnetic centers N_{PC} is equal to about 3.4×10^{22} at $T = 305$ K which is by one order larger than at $T = 4.2$ K and thus impossible.

Thus, H_1 does not depend on temperature and, therefore, the C–W paramagnetism is not justified by the temperature dependence of H_1 at a magnetic field of $H = 8$ T. The only kind of paramagnetic system with a linear function $M(H)$ and not dependent on T is the Van Vleck paramagnetism [10]. In this case, $M = \chi_{V-V}\cdot H = N\alpha H$ where $\alpha = \mu_B^2\ \Sigma_n(|<0|J|n>|^2/\Delta_{n0})$ is the virtual transitions of the angular moment between the atomic multiplet levels if $\Delta_{n0} >> kT$. All iron atoms take part in the formation of the Van Vleck paramagnetic susceptibility. At smaller fields, the C–W paramagnetic susceptibility becomes actual.

Using the above determinations, we can find the concentration of superparamagnetic clusters, N_{cl}, and the average number of paramagnetic atoms in the clusters, n_s, for steels CN1.07, CN0.85, and C1.2:

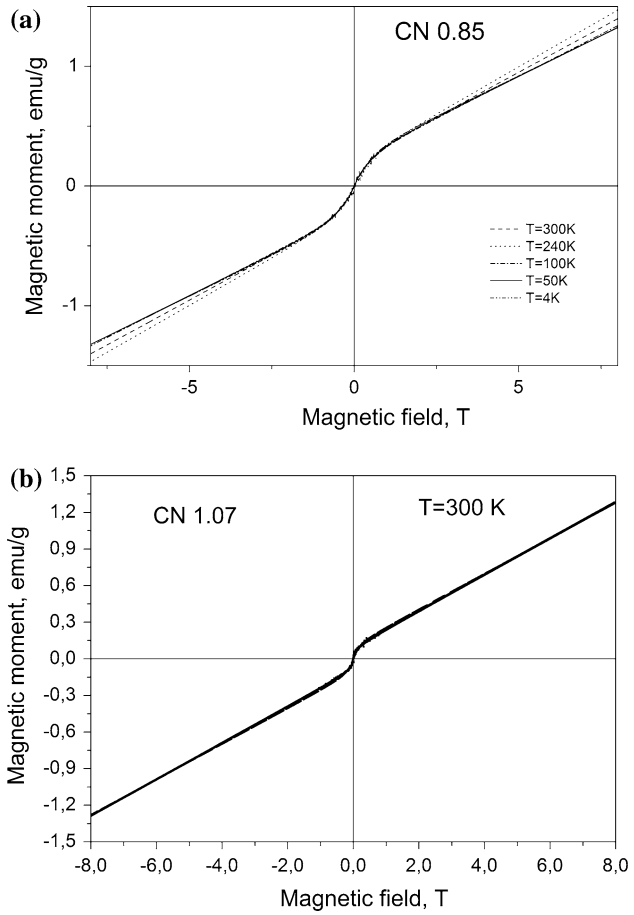

Fig. 6 Magnetic moment versus magnetic field in steel CN0.85 at different temperatures (**a**). Fitted magnetic moment curves at 305 K are presented for steels CN1.07 (**b**) and CN0.85 (**c**)

Table 3 Parameters in formula (11) for magnetization curves

Steel	T, K	M_0, emu/g	H_0, T	H_1, T
CN1.07	300	0.12	0.08	7
CN0.85	300	0.22	0.2	6.7
CN0.85	240	0.23	0.2	6.5
CN0.85	100	0.23	0.2	7.1
CN0.85	50	0.22	0.15	7.1
CN0.85	4	0.24	0.2	7.2
C1.2	300	0.01	0.01	5.0

$$\begin{aligned} \text{CN1.07}: &\quad N_{\text{cl}} = 4.6 \cdot 10^{19}\text{cm}^{-3}, \quad n_{\text{s}} = 2,570; \\ \text{CN0.85}: &\quad N_{\text{cl}} = 8.4 \cdot 10^{19}\text{cm}^{-3}, \quad n_{\text{s}} = 1,012; \\ \text{C1.2}: &\quad N_{\text{cl}} = 3.5 \cdot 10^{18}\text{cm}^{-3}, \quad n_{\text{s}} = 2 \cdot 10^{4}. \end{aligned} \tag{12}$$

The size of the superparamagnetic clusters can be estimated using the number of paramagnetic atoms in the cluster, n_{s}. According to the obtained data, steel CN1.07 is characterized by a low concentration of clusters, N_{cl}, with a size of about 5 nm, whereas N_{cl} in steel CN0.85 is higher, however, the clusters have a smaller size of about 3.5 nm. The obtained data are consistent with those of CESR and indicate a decrease of chemical nonhomogeneity in CrMnCN austenitic steels with decreasing C/N ratio

The carbon steel C1.2 is characterized by the smallest concentration of superparamagnetic clusters which have the largest size of about 8 nm.

Small angle neutron scattering

In contrast to magnetization, the measurements of SANS give information on the chemical nonhomogeneity. Figure 7 shows the differential cross section of neutron scattering as a function of the scattering vector in the studied steels. The scattering values are given in cm^{-1}, i.e. in absolute units. With this aim, a standard calibration of the instrument was carried out using the scattering on a non-coherent specimen, in this case on water.

In general, the CN steels are nearly homogeneous on a mesoscopic scale, whereas the carbon Hadfield steel C1.2, used for comparison, reveals a much higher nonhomogeneity of concentration.

The scattering data of steel CN0.96 are given in Fig. 8 in Guinier co-ordinates of the logarithmic intensity versus q^2. The fitting was carried out on six smallest values of transferred impulses. Assuming a spherical geometry of the nonhomogeneities, their size was determined at $R_0 \approx 10$ nm with an error of about 30%. Nearly the same results were obtained for steels CN1.07 and CN 0.85.

The much higher scattering of steel C1.2 is characterized by a power impulse dependence, $I \sim q^n$, where $n \approx -2.85$, which is typical for volume fractal structures. In this case, the maximum size of nonhomogeneities of

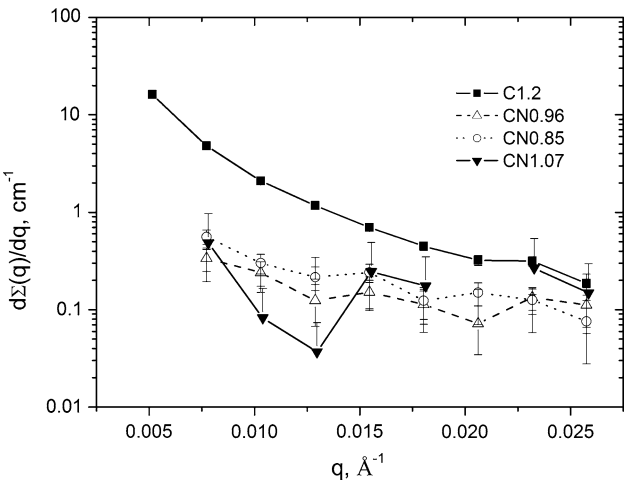

Fig. 7 Differential cross section of small angle neutron scattering dΣ(q)/dq in steels CN1.07, CN0.96, CN0.85, and C1.2 as a function of the scattering vector **q**

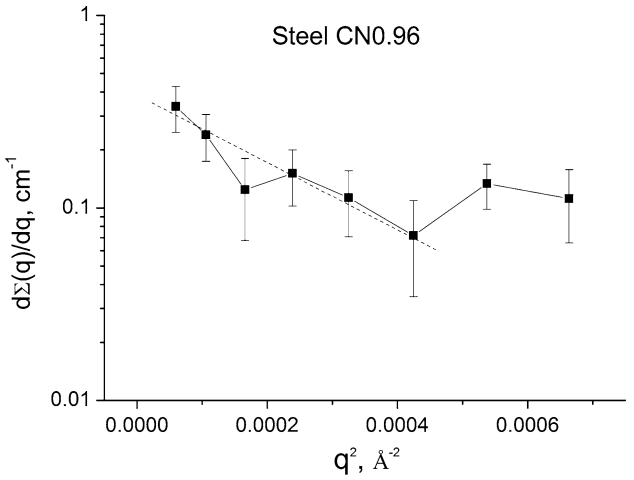

Fig. 8 Differential cross section of small angle neutron scattering dΣ(q)/dq in steel CN0.85 in Guinier co-ordinates

concentration was obtained from the instrument resolution, $q_{\min} \leq 3 \times 10^{-2}\ \mathrm{nm}^{-1}$. Correspondingly, the size of inhomogeneities $R_{\max} \geq (1/q_{\min})$ is equal to about 30 nm.

The comparison of these data with those of CESR and magnetization shows that the size of chemical clusters is a bit larger than that of the superparamagnetic ones.

Stacking fault energy as a tool for estimation of concentration nonhomogeneity

Using local X-ray emission spectroscopy, the short-range decomposition in neutron- and electron-irradiated CrNi austenitic steels was studied in [11, 12]. It was shown that, with a modulation wave of about several microns, the areas enriched in iron and chromium alternate with those enriched in nickel. As the electron irradiation does not change the atomic interactions and only, due to enhanced diffusion, assists thermodynamic equilibrium, it is clear that the atomic distribution in austenitic steels is far from an ideal solid solution.

In the present study, complementarily to the above-described experiments, we used measurements of SFE in order to obtain information on the effect of carbon + nitrogen or carbon on the chemical nonhomogeneity of austenitic steels. Such measurements are also useful for testing a possible correlation between the electron structure and SFE in view of the data in [13] where an inverse correlation was observed between SFE and the density of electron states at the Fermi level in pure metals.

The results of measuring the dislocation splitting are shown in Fig. 9 and the obtained values of the dislocation

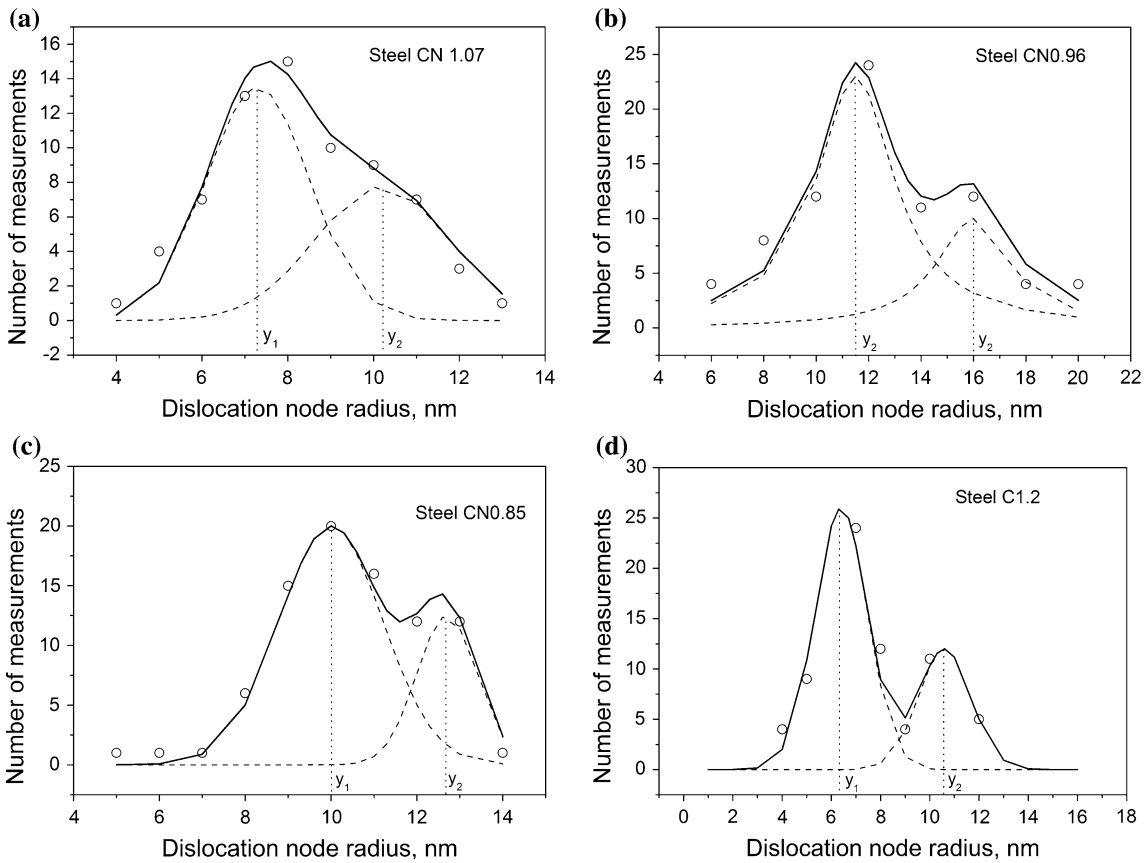

Fig. 9 Frequency curves of the measured dislocation node radius in austenitic steels: **a** CN1.07, **b** CN0.96, **c** CN0.85, and **d** C1.2

Table 4 Dislocation node radius, y, and SFE

Steel	y_1, nm	y_2, nm	SFE_1, mJ/m^2	SFE_2, mJ/m^2	ΔSFE, mJ/m^2
CN1.07	7.3	10.2	59	43	17
CN0.96	11.5	16.0	38	27	11
CN0.85	10.0	12.0	43	36	7
C1.2	6.4	10.6	68	41	27

node radius and SFE are presented in Table 4. The two maxima of dislocation splitting in Fig. 9 give evidence of short-range decomposition in the studied steels. The fitting of the experimental data was carried out using the Gauss distribution, which is natural for the statistical scattering of the experimental data. One can see from Table 4 that the homogeneity of the solid solution, estimated from ΔSFE, is improved by a decreasing content of carbon in the CN steels and consequently by a decreasing C/N ratio. It is significantly worse in the carbon steel C1.2.

The obtained values of SFE in CrMnCN steels are presented in Fig. 10 along with the data of the conduction electron concentration which is proportional to the density of electron states at the Fermi level, $D(E_F)$. Both SFE_1 and SFE_2 are inversely proportional to the concentration of conduction electrons, which is consistent with the tendency observed in [13] for pure metals. It is relevant to note that the same inverse relation between SFE and $D(E_F)$ was observed in [14] for austenitic CrMn steels with nitrogen, whereas a direct proportionality occurred in steels additionally alloyed with nickel.

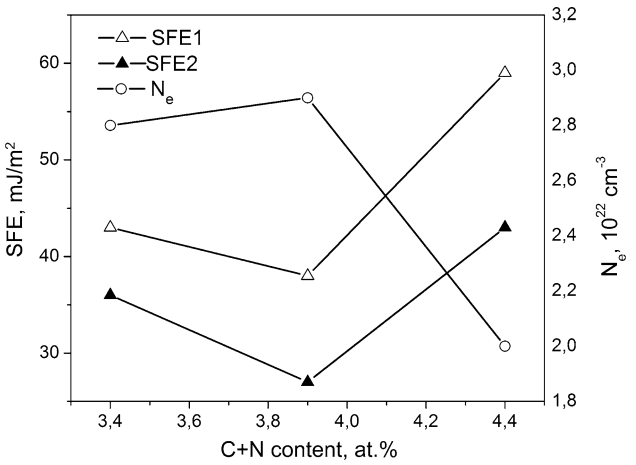

Fig. 10 Stacking fault energies and concentration of conduction electrons in CrMnCN steels versus C + N content in at.%

Discussion

The main question is how the C/N ratio of austenitic CrMnCN steels affects their chemical homogeneity. The following analysis can be made based on the results obtained by measuring the electron spin resonance, magnetization, small angle neutron scattering, and stacking fault energy.

In comparison with nitrogen steels studied in [1, 2], the carbon + nitrogen ones are characterized by an increase in the concentration of free electrons. This enhancement of the metallic character of interatomic bonds is obviously responsible for a higher impact toughness of C + N steels and a decrease in the temperature of ductile-to-brittle transition, as obtained in [15].

The data presented in Table 2 show that the concentration of free electrons generally increases with a decreasing C/N ratio, also there is no remarkable difference between steels CN0.96 and CN0.85, which points to some optimum of the C/N ratio. The data of CESR (Sect. 3.3.2) and magnetization (Sect. 4) show also that, with a decreasing C/N ratio, the density of clusters increases, whereas their size decreases. In other words, the atomic distribution becomes more homogeneous, which suggests a tendency to the short-range atomic ordering. This result is consistent with earlier data on the correlation between the metallic character of interatomic bonds and atomic distribution in austenitic steels with nitrogen or carbon [16] and allows to suggest that, at an appropriate C/N ratio, the alloying with carbon + nitrogen should increase thermodynamic stability of austenitic steels. As an indirect confirmation of this, one can refer to the data [17] on the martensitic steel of Cronidur-30 type containing (mass%) 15Cr, 1.0Mo and 0.6C or 0.62N or 0.29C + 0.35N. After an equal solution treatment at 1,100 °C and quenching in water, the substitution of carbon by nitrogen increased the fraction of retained austenite from 27 to 51%, whereas 71% of retained austenite was obtained in the case of combined alloying with C + N.

A correlation between the atomic interaction and atomic distribution is also confirmed by the markedly increased size of clusters in Hadfield steel C1.2 (see the data of magnetization in Sect. 4 and SANS in Sect. 5) in combination with the absence of a CESR signal in this steel, which gives evidence of an extremely low concentration of free electrons. As a result, the Hadfield steel has a rather low stability in relation to precipitation at low temperature heating in comparison with austenitic steels containing nitrogen or carbon + nitrogen.

In view of the low concentration of free electrons in Hadfield steel, i.e. the prevailing covalent character of interatomic bonds, a special comment can be given in relation to its good impact toughness, though it is smaller in comparison with austenitic steels containing nitrogen or carbon + nitrogen (see, e.g. [15]). The stacking fault

energy of about 50 mJ/m^2 of C1.2 (see [18]), which is not favorable for strain-induced $\gamma \rightarrow \varepsilon$ transformation. The decrease in dislocation mobility due to carbon-enhanced covalent bonds, which locally increases the shear modulus within the carbon clouds around dislocations, should create appropriate conditions for the extremely intensive twinning in cold-worked Hadfield steel. In fact, this steel is a good example of the TWIP effect, which is the true reason for its tough mechanical behavior. As shown in [18], such an intensive twinning is not observed in austenitic steels containing nitrogen or carbon + nitrogen.

The discrepancy between the data of cluster size obtained by CESR, magnetization, and by SANS needs special comments. According to the CESR and magnetization data, the size of clusters is changed from 5 nm in steel CN1.07 to 3 nm in CN0.85. SANS measurements give a size of about 10 nm with an error of nearly 30% for all CN steels and about 30 nm for steel C1.2.

It should be noted that the resolution limit for SANS in relation to chemical nonhomogeneity amounts to about 5 nm and, as follows from Fig. 7, the error of measurement for CN steels is rather large. Thus, the difference between the data for CN steels obtained from magnetic measurements and those using SANS could be related to the errors in determining a cluster size near the limit of SANS resolution. However, the discrepancy between the size of clusters in Hadfield steel, as obtained from SANS and magnetic measurements, cannot be explained so easily.

One reason may be the difference in the local enrichment of substitutional solutes in superparamagnetic clusters and zones of enhanced neutron scattering. The exchange interaction between Mn and Cr atoms is sufficiently strong to polarize magnetic moments, i.e. to form superparamagnetic clusters, but weakens as the concentration of these elements decreases at the periphery of chemical nonhomogeneities. At the same time, an enrichment in Mn and Cr can be sufficient for an enhanced scattering of neutrons beyond the limits of superparamagnetic clusters.

Finally, let us discuss the applicability of SFE measurements for the estimation of chemical nonhomogeneities in solid solutions. The distance between the frequency maxima of the triple node radius in Fig 9, see also ΔSFE in Table 4, decreases with a decreasing C/N ratio points to a higher homogeneity, which is consistent with the data of concentration nonhomogeneities obtained using other experimental methods.

Conclusions

1. A high concentration of conduction electrons is obtained in the austenitic CrMnCN steels CN1.07, CN0.96, and CN0.85, which evidences an enhanced metallic character of interatomic bonds. It is impossible, though, to obtain a signal of conduction electrons in the MnC Hadfield type steel C1.2 because of their low concentration.
2. The temperature dependence of the resonance magnetic field of CESR indicates the presence of superparamagnetic clusters (clusters of atoms with a large total magnetic moment) which, in fact, are the clusters of Cr and Mn atoms. In consistency with CESR data, the magnetic measurements show that steel CN1.07 has a lower concentration of clusters in comparison with steel CN0.85, however, the clusters in the latter have a smaller size indicating that the chemical nonhomogeneity decreases with a decreasing C/N ratio.
3. According to the data of small angle neutron scattering, the chemical nonhomogeneity of the CrMnCN steels is nearly the same with an error of about 30% but it is much higher in the MnC steel.
4. According to the EPR data, a striking change of magnetic properties occurs in steel CN0.85 at temperatures below 86 K. The absorption of the microwave power signal demonstrates a large dispersion, which indicates a large spreading of the magnetic moments and orientations of superparamagnetic moments due to local magnetic fields caused by superparamagnetic clusters. Based on the measurements of static magnetization, this phenomenon was interpreted in terms of blocking of the superparamagnetic moments.
5. Using TEM, two maxima of dislocation splitting are obtained, which correspond to two different values of the stacking fault energy. This result suggests that the chemical homogeneity is improved as the C/N ratio decreases, which is consistent with the data obtained using other experimental methods. An inverse proportionality is found between the stacking fault energy and the concentration of conduction electrons in the CrMnCN steels.

References

1. Gavriljuk VG, Efimenko SP, Smouk YeE, Smouk SYu, Shanina BD, Baran NP, Maximenko VM (1993) Phys Rev B 4:3224
2. Shanina BD, Gavriljuk VG, Konchitz AA, Kolesnik SP, Tarasenko AV (1995) Phys Stat Sol a 149:711
3. Berns H, Duz' VA, Ehrhardt R, Gavriljuk VG, Petrov YuN, Tarasenko AV (1997) Z Metallk 88(2):109
4. Shanina BD, Gavriljuk VG, Konchitz AA, Kolesnik SP (1998) J Phys Condens Matter 10:1825
5. Gavriljuk VG, Shanina BD, Berns H (2008) Acta Mater 56:5071
6. Ruff AW Jr (1970) Metall Trans A 1:2391

7. Feher G, Kip A (1955) Phys Rev 98:337
8. Pifer JH, Magno R (1971) Phys Rev B 3:663
9. White RM (1983) Quantum theory of magnetism. Springer-Verlag, Berlin, New York
10. Vonsovsky SV (1971) Magnetism. Nauka, Moscow (in Russian)
11. Garner FA, McCarthy JM (1990) In: Russel KC, Smith DF (eds) Physical metallurgy of controlled expansion invar-type alloys. TMS-AIME, Warendale, PA, pp 187–206
12. Rotman F, Gilbon D, Lorant H, Dimitrov O (1987) Mater Sci Forum 15–18:1409
13. Noskova NI, Pavlov VA, Nemnonov SA (1965) Phys Met Metallogr 20:920 (in Russian)
14. Gavriljuk V, Petrov Yu, Shanina B (2006) Scripta Mater 55:537
15. Berns H, Gavriljuk VG, Riedner S, Tyshchenko AI (2007) Steel Res Intern 78:710
16. Gavriljuk VG, Shanina BD, Berns H (2000) Acta Mater 48:3879
17. Berns H, Duz VA, Ehrhardt R, Gavriljuk VG, Tarasenko AV (1995) Met Phys Adv Technol 15:561
18. Gavriljuk VG, Tyshchenko AI, Bliznuk VV, Yakovleva IL, Riedner S, Berns H (2008) Steel Res Int 79:413